Journal of
Composites Science

MDPI

Article

Supplementary Cementitious Material from Epsom Salt Production Waste

Rimvydas Kaminskas *, Arijus Zuzevicius and Irmantas Barauskas

Department of Silicate Technology, Faculty of Chemical Technology, Kaunas University of Technology, Radvilenu 19, LT-50254 Kaunas, Lithuania; arijus.zuzevicius@ktu.edu (A.Z.); irmantas.barauskas@ktu.lt (I.B.)
* Correspondence: rimvydas.kaminskas@ktu.lt; Tel.: +370-62023774

Abstract

In this study, the potential use of Epsom salt production waste as a supplementary cementitious material was investigated. This acidic waste was neutralized with lime milk and used to replace up to 25 wt.% of Portland cement. The following research methods were employed: XRD, XRF, SEM, DSC-TG, and isothermal calorimetry. The waste neutralization process was found to proceed consistently, producing a neutral material (pH = 7.5) composed of amorphous silicon compounds with a negligible impurity of crystalline antigorite. Consequently, this material exhibits very high pozzolanic activity. The neutralized Epsom salt production waste accelerates the early hydration of Portland cement and promotes an intense pozzolanic reaction. This new material is a highly effective supplementary cementitious material, capable of replacing up to 25 wt.% of Portland cement without reducing its strength class.

Keywords: Epsom salt; waste; pozzolana; Portland cement; hydration

check for updates

Academic Editor: Siqi Ding

Received: 20 November 2025
Revised: 9 December 2025
Accepted: 16 December 2025
Published: 18 December 2025

Citation: Kaminskas, R.; Zuzevicius, A.; Barauskas, I. Supplementary Cementitious Material from Epsom Salt Production Waste. *J. Compos. Sci.* **2025**, *9*, 708. https://doi.org/10.3390/jcs9120708

Copyright: © 2025 by the authors. Licensee MDPI, Basel, Switzerland. This article is an open access article distributed under the terms and conditions of the Creative Commons Attribution (CC BY) license (https://creativecommons.org/licenses/by/4.0/).

1. Introduction

Ordinary Portland cement (OPC) production accounts for nearly 7% of global CO_2 emissions, primarily due to the decomposition of limestone during the formation of clinker and the combustion of fuels, as well as the extensive use of natural raw materials [1]. Waste utilization—be it supplementary cementitious materials (SCMs), incorporated into raw feed, or co-processed in rotary kilns—offers a means to reduce clinker costs, lower the carbon intensity of cement production, and promote circular economy practices [2–4]. However, the practical implementation of these strategies remains limited by several factors, including fluctuations in waste composition, the presence of harmful impurities such as chlorides and heavy metals, and other related challenges [1,5].

The main waste streams used include coal fly ash, ground granulated blast furnace slag, glass waste, municipal solid waste incineration ash, red mud, phosphogypsum and other industrial residues [2,3,6–8]. It is well established that many materials used as SCMs enhance the mechanical strength and durability of Portland cement paste, as well as improve resistance to chloride ingress and sulfate attack, while reducing permeability [9–12]. These materials are employed not only for the beneficial properties they impart to the cement matrix, but also because large quantities of such waste are accumulated globally.

Cement plants can use smaller quantities globally, but sufficient amounts of waste are generated in local areas near the plants. This could be waste such as rice husk ash, spent catalytic cracking catalyst, construction and demolition waste, and other waste [13–15].

Additionally, small amounts of Portland cement can be replaced with synthetic materials from waste or inexpensive raw materials [16,17].

There are wastes from other industrial sectors that have been scarcely studied. One such waste is Epsom salt production waste.

Epsom salt is usually produced by treating silicate minerals with a high concentration of magnesium, usually olivine [$(Mg,Fe,Ni)_2SiO_4$] or serpentinite [$Mg_3Si_2O_5(OH)_4$] with sulfuric acid (H_2SO_4). The production of magnesium hydroxide from serpentinite is described by the following chemical reactions [18]:

$$Mg_3Si_2O_5(OH)_4 + 6H_2SO_4 \rightarrow 3Mg(HSO_4)_2 + 2SiO_2 + 5H_2O$$

$$Mg(HSO_4)_2 + 4NaOH \rightarrow Mg(OH)_2\downarrow + 2Na_2SO_4 + 2H_2O$$

This process produces a suspension with a high concentration of magnesium sulfate ($MgSO_4$) that contains solid residues, most of which are amorphous silica SiO_2 and other undissolved mineral fractions.

The production of $MgSO_4$ from magnesium silicates results in several primary waste streams, including a relatively Fe-rich sludge, a silica-rich residue and an acidic effluent. Upon neutralization with MgO or NaOH, Fe^{2+} is oxidized to Fe^{3+} and precipitated as $Fe(OH)_3$ or goethite (FeO(OH)) at pH 6–7. This sludge also contains traces of Ni, Cr, and other heavy metals. The undissolved silicate matrix, with its high silica content, is separated by filtration.

Resource utilization initiatives aim to convert waste into valuable products. Iron-rich sludge can be processed into magnetite (Fe_3O_4), which can be used in the production of iron and steel by magnetic separation, or as an adsorbent in wastewater treatment, effectively removing As, Cr and phosphates [19,20].

The situation with colloidal silica is somewhat different. First, colloidal silica complicates the filtration process and reduces the amount and purity of magnesium sulfate [18]. Second, due to its amorphous nature, silica adsorbs on the surface sulfuric acid and remains acidic, with a pH of 3–4. Due to this characteristic, this SiO_2-rich waste cannot be used directly in the cement or building materials industry. However, the various varieties of amorphous silica are a very valuable addition to Portland cement.

Sources of amorphous silica include natural materials such as volcanic ash, tripoli, opoka (natural pozzolans), industrial by-products such as silica fume, and synthetic compounds obtained from minerals such as olivine [21–23]. When incorporated as a supplementary cementitious material (SCM), amorphous silica exhibits pozzolanic behavior by reacting with calcium hydroxide produced during cement hydration, resulting in the formation of additional calcium silicate hydrate (C–S–H). This reaction improves the mechanical strength and durability of concrete [24]. Therefore, the objective of this work is to determine the possibility of using amorphous silica-rich Epsom salt production waste as new SCM and to investigate its influence on the characteristics of Portland cement.

2. Materials and Methods

Epsom salt production waste (ESW), collected during the production of Epsom salt and Portland cement CEM I 42.5 N (OPC), was used. The chemical compositions of ESW and cement are presented in Table 1.

Calcium oxide was obtained by calcining $CaCO_3$ (Sigma-Aldrich, Steinheim, Germany) at a temperature of 950 °C for 1 h. The specific surface area and the quantity of free CaO were equal to S_a = 625 m^2/kg and 98.9 wt.%, respectively.

Table 1. Chemical composition of raw materials.

Component (wt.%)	ESW	OPC
SiO_2	88.35	19.72
Al_2O_3	0.10	4.93
Fe_2O_3	2.47	3.25
CaO	0.48	61.19
MgO	2.64	3.93
K_2O	-	1.04
Na_2O	-	0.14
Cr_2O_3	0.07	-
NiO	0.12	-
SO_3	2.73	2.6
P_2O_5	0.83	-
MnO	0.05	-
Other	2.16	3.2
Specific surface area, m^2/kg	320	320

XRD analysis data (Figure 1a) show that ESW consists only of amorphous materials (hump at 15–40 2θ) with crystalline antigorite (PDF 04-015-5514) and magnetite (PDF 04-008-4511) impurities.

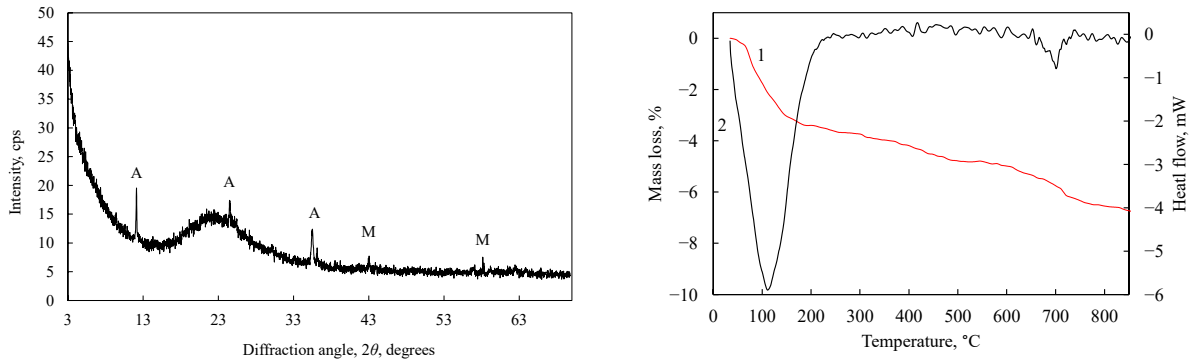

(**a**) (**b**)

Figure 1. (**a**) X-ray diffraction patterns of ESW. Indexes: A, antigorite ($Mg_3(Si_2O_5)(OH)_4$); M, magnetite (Fe_3O_4). (**b**) Simultaneous thermal analysis (1—TG; 2—DSC) outcome of ESW.

In the DSC curve of the ESW sample (Figure 1b), an endothermic peak appears around 115 °C, corresponding to the release of physically adsorbed water. Another endothermic peak, observed near 700 °C, is associated with the thermal decomposition of antigorite [25]. The accompanying thermogravimetric (TG) analysis shows an overall weight loss of approximately 7.0 wt.%.

Because ESW has an irregular particle size distribution, it was milled to a specific surface area equal to 320 m^2/kg, with a mean particle diameter of 31.69 µm (Figure 2).

SEM images show (Figure 3) that ESW consists of irregularly shaped sharp-edged particles. Meanwhile, the ground material also contains irregularly shaped but partially rounded particles.

Neutralization of ESW. For the neutralization of acid rests, 20 g of ESW was mixed with water to obtain three different water/solid material (W/S) ratios—1.25; 2.5 and 5.

Then, the obtained waste pulp was transferred to a container with a 90 rpm propeller mixer. Later, lime milk was gradually dripped into this mixer. The process continued until the waste pulp was fully neutralized and the pulp pH = 7.5 was reached. The neutralized pulp was then filtered and dried in a dryer for 24 h at 70 °C.

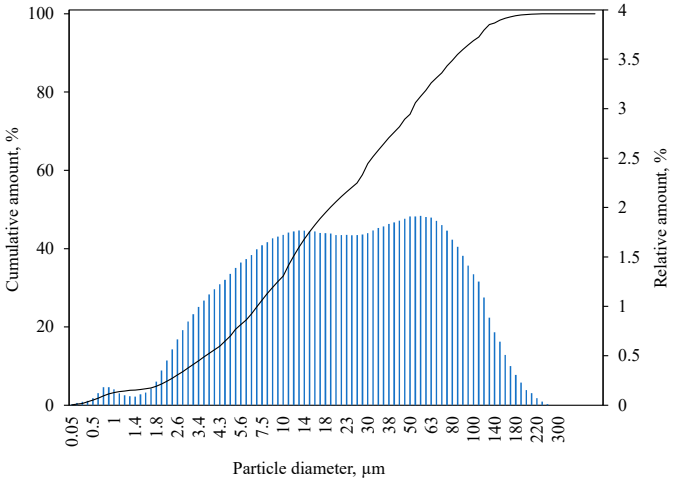

Figure 2. Particle size distribution of ESW.

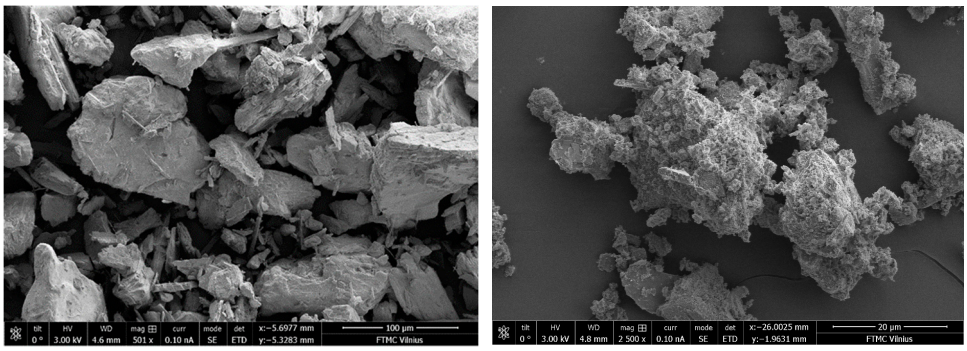

(**a**) (**b**)

Figure 3. SEM images of ESW (**a**) as received; (**b**) additionally milled.

Lime milk preparation. Lime milk was prepared at a concentration of 3.5%, that is, 35 g. CaO was dissolved in a liter of deionized water.

Simultaneous thermal analysis (STA) was carried out using a PT1000 analyzer (Linseis, Selb, Germany) over a temperature range of 30–1000 °C, with a heating rate of 15 °C min^{-1}.

X-ray diffraction (XRD) measurements were conducted with a Bruker D8 Advance (Bruker AXS, Karlsruhe, Germany) diffractometer employing Bragg–Brentano geometry, using a step size of 0.02° and a 2θ scan range between 3° and 70°.

The X-ray fluorescence (XRF) data were collected on a Bruker S8 Tiger WD (Bruker AXS, Karlsruhe, Germany) spectrometer. The data were analyzed using SPECTRAPlus V. 2 QUANT EXPRESS software.

The materials' particle size distribution and specific surface area were analyzed using a CILAS 1090 LD particle analyzer, capable of measuring within the 0.04–500 µm range.

An FEI Helios Nanolab 650 scanning electron microscope (SEM) equipped with an energy-dispersive X-ray spectrometer (Oxford Instruments, High Wycombe, UK, INCA 4.15 software) was used for the surface investigation of the samples.

The influence of neutralized ESW on the properties of Portland cement was evaluated by substituting 5, 15 and 25 wt.% of OPC with the obtained additive.

The properties of cement paste were ascertained based on EN 196-3 [26].

For instrumental analysis, sand-free ordinary Portland cement (OPC) paste was produced. The samples were submerged in distilled water maintained at 20 ± 1 °C for curing durations of 2, 7 and 28 days. After each period, the specimens were ground, washed with isopropyl alcohol, dried at 45 °C for 12 h, and preserved in airtight containers.

Samples (prisms 40 × 40 × 160 mm) for compressive strength analysis were formed in accordance with EN 196-1 [27]. The cement–sand ratio in the samples was 1:3 and the water–cement ratio was 0.5:1.

Isothermal calorimetry (IC) was performed with a TAM Air III calorimeter, TA Instruments, Eschborn, Germany. The temperature of the experiment was 25 ± 0.1 °C. An amount of 3 g of cement was mixed with deionized water to obtain a water-to-solid ratio of 0.5, without prehydration of the samples. The measured heat was normalized per gram of Portland cement.

The pH values of the solution were measured with a pH meter, inoLab pH 30 (WTW, Weilheim, Germany). The accuracy was ±0.01 pH units

Pozzolanic activity was measured in accordance with the NF P18-513 standard [28].

3. Results

3.1. Neutralization of ESW

In this work, we was decided to neutralize the acidic ESW residues with lime milk. This method was chosen because sulfuric acid residues can react with calcium hydroxide, forming dihydrate gypsum according to the following chemical reaction:

$$Ca(OH)_2 + H_2SO_4 \rightarrow CaSO_4 \cdot 2H_2O$$

The dihydrate gypsum that can form during this reaction is a harmless material that is used in cement production as a setting time regulator. To evaluate the course of the neutralization process, ESW with different W/S ratios was used. The results of the studies are presented in Figure 4.

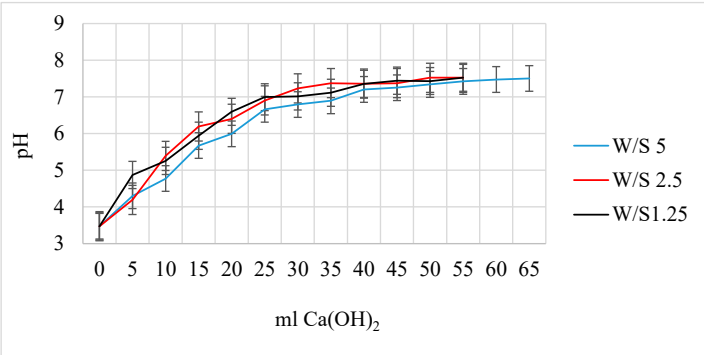

Figure 4. ESW neutralization curves.

The studies demonstrate that the ESW neutralization process consistently occurs, and the ratio of water-to-solid material (W/S) has a negligible effect on the overall neutralization outcome. However, a higher W/S ratio slows the pH increase and extends the neutralization time: 23 min at W/S 1.25, 35 min at W/S 2.5, and 55 min at W/S 5.

The XRD analysis of neutralized ESW (NESW) samples (Figure 5) showed that the W/S ratio has no effect on the neutralization process, because the mineral composition of the samples is identical. Also, all XRD curves of NESW are very similar to those of raw ESW, except the peaks of magnetite disappear (due to dissolution under alkaline conditions) and those of antigorite decrease slightly.

Analogously, the STA curves and SEM images are similar, so only the NESW is given (Figure 6), with a W/S of 2.5.

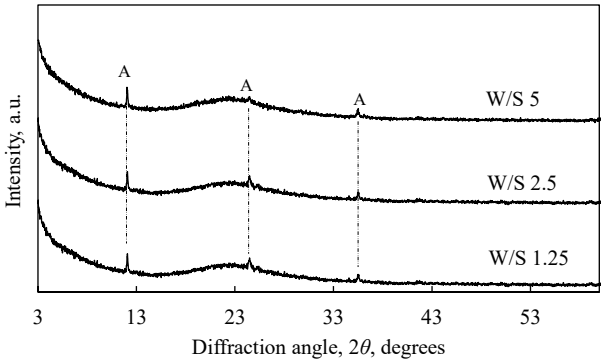

Figure 5. X-ray diffraction patterns of ESW after neutralization. Indexes: A, antigorite ($Mg_3(Si_2O_5)(OH)_4$).

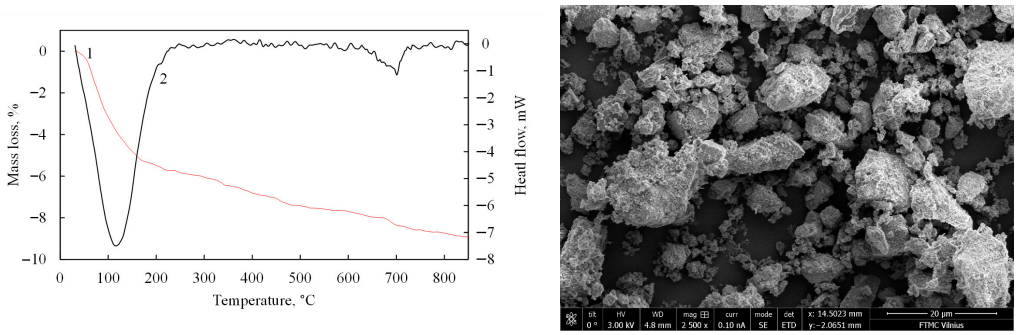

Figure 6. NESW when W/S = 2.5: (**a**) STA curves (1—TG; 2—DSC); (**b**) SEM image.

As well as in the case of raw ESW, two endothermic peaks are observed in the DSC curve (Figure 6a) at 115 and 700 °C that show the removal of adsorbed moisture and the decomposition of antigorite, respectively. The only difference is that during antigorite decomposition, a slightly lower mass loss (0.62%) was recorded in the TG curve of the neutralized sample than in TG curve of the raw ESW (0.91%). Also, after neutralization, the particle shape does not change (Figure 6b) because the sample is dominated by irregularly shaped, partially rounded particles.

The chemical compositions of NESW after neutralization with different W/S ratios are presented in Table 2.

Table 2. Chemical compositions of NESW with different W/S ratios.

Component (wt.%)	ESW	NESW; W/S = 1.25	NESW; W/S = 2.5	NESW; W/S = 5
SiO_2	88.35	92.25	92.15	92.47
Al_2O_3	0.10	0.12	0.13	0.13
Fe_2O_3	2.47	0.86	0.93	0.90
CaO	0.48	0.56	0.55	0.58
MgO	2.64	1.52	1.51	1.51
Cr_2O_3	0.07	0.07	0.06	0.06
NiO	0.12	0.06	-	0.08
SO_3	2.73	0.84	0.76	0.76
P_2O_5	0.83	0.56	0.55	0.52
Other	2.21	3.16	3.36	2.99

As expected, as the W/S ratio increases, a lower amount of SO_3 remains in the NESW material. However, this difference is negligible. The amount of P_2O_5 is also reduced, but the amount of P_2O_5 remaining in the neutralized material does not depend on the W/S ratio. The amounts of these two oxides are reduced because they are the most soluble

components. The decrease in the content of MgO and Fe_2O_3 is related to the decrease in the amount of antigorite in the NESW and the transition of Fe_2O_3 into the liquid phase, as shown in Figures 4 and 5. The decrease in the amount of both of these components is also independent of the W/S ratio.

In summarizing the results of the studies in this section, it can be stated that ESW can be neutralized with lime milk, and the water/solid material (W/S) ratio does not have a decisive influence on the neutralization process. During neutralization, acidic components are bound to neutral compounds. These compounds do not settle on the surface of the ESW material, but pass into the liquid medium because they have not been identified in the NESW material by the XRD and STA methods. Due to the low concentration of newly formed compounds (gypsum and others) in the liquid medium, they do not crystallize, so this medium can be reused for neutralization, supplemented with lime milk to the required pH. Therefore, for industrial applicability and economic and ecological reasons, NESW was chosen for the following studies, neutralized for 23 min when W/S was 1.25.

3.2. Influence of ESW on OPC Characteristics

The pozzolanic activity of NESW was determined. It was established that NESW is characterized by very high pozzolanic activity. The pozzolanic activity of ground NESW reached 1085 mg CaO/g, which is similar to or higher than the activity value of metakaolinite, as estimated by the same method [29].

Subsequently, the effect of NESW on the characteristics of cement paste was evaluated. Test samples were made by substituting 5–25 wt.% of OPC with the NESW additive. The influence of NESW on the normal consistency and setting time of the OPC paste is presented in Table 3.

Table 3. The effect of NESW on cement paste properties.

Component (wt.%)		Abbreviation	Normal Consistency W/C (%)	Setting Time (min)	
OPC	**NESW**			**Initial**	**Final**
100	-	OPC	0.27	84	126
95	5	S5	0.28	82	115
85	15	S15	0.30	80	105
75	25	S25	0.32	75	100

The addition of the NESW additive led to a slight increase in water demand to reach normal consistency in the cement paste. This effect was related to the absorption of some of the water for the wetting of the NESW particles. The shorter binding duration may also have been related to the nature of NESW. Amorphous NESW particles have very strong adsorptive properties, and this process continued after the cement powder was mixed with water and the cement paste was formed. This way, part of the water required for cement hydration was consumed, and less water meant faster stiffening, shortening the duration of the initial and final sets.

The influence of NESW on the early hydration of cement paste was determined by isothermal calorimetry (IC) tests. The results of the test are shown in Figure 7.

Two peaks of heat evolution were observed on the calorimetric curve of the samples: the first concerned wetting a cement powder and the second related to the hydration of the deeper layers of calcium silicates. On the second peak, there is a visible shoulder on the so-called Sulfate depletion peak. This shoulder is associated with a further dissolution of tricalcium aluminate and the formation of ettringite [30–32]. It is slightly more intense in samples with additives, as NESW contains additional amounts of both SO_3 and Al_2O_3. In samples with additives, the induction period (Figure 7a) lasts longer (2 h 15 min–3 h) than in the OPC sample (2 h 10 min), but during this period, samples with additives release

more heat (Figure 7b). During the second exothermic reaction stage, the heat flow curve showed that the NESW-containing samples exhibited earlier heat release compared to the OPC sample. The sample with 15 wt.% NESW reached its maximum heat flow 8 h 50 min after the hydration began, while the sample with 25 wt.% NESW reached its maximum at 8 h 25 min. On the contrary, both the pure cement and the sample with 5 wt.% NESW achieved their maximum heat flow at 9 h 12 min. Additionally, at up to 20 h of hydration, all samples with the NESW additive emitted more hydration heat than OPC. Therefore, it can be inferred that the addition of NESW enhanced the rate of early-stage cement hydration.

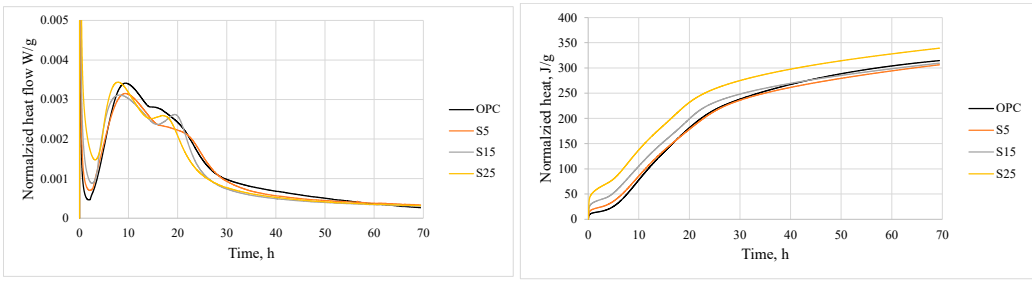

(**a**) (**b**)

Figure 7. The IC tests results: (**a**) heat flow; (**b**) total heat.

Figure 8 shows the compressive strength data of the OPC with different amounts of NESW. After 2 days of hardening, the highest compressive strength was shown for the OPC and S5 sample (~20 MPa). Although the S15 and S25 samples exhibited lower compressive strength values, all specimens achieved strengths above 10 MPa, satisfying the requirements of the EN 197-1:2011 standard [33]. The lower compressive strength of the S15 and S25 samples is related to the fact that a significantly lower amount of OPC was hydrated in these samples. Furthermore, at this stage of hardening, a possible pozzolanic reaction has usually only just begun and the number of new hydrates formed does not compensate for the influence of conventional cement hydrates on the compressive strength of the samples.

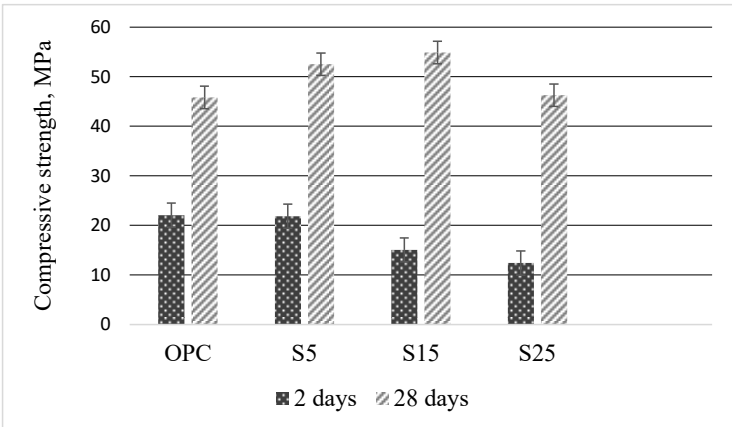

Figure 8. The compressive strength of the samples hardened for 2 and 28 days.

After 28 days of curing, all samples with the NESW additive exhibited a higher compressive strength (46.3–54.9 MPa) compared to the OPC sample (45.8 MPa). The S15 sample is characterized by a particularly high compressive strength (54.9 MPa), which corresponds to an even higher strength class (52.5) than the class of OPC used (42.5). Thus, NESW is a very effective SCM, and it can replace as much as 25 wt.% of Portland cement.

The XRD curves (Figure 9) indicate that no new crystalline phases were detected in the samples containing the NESW additive after 7 and 28 days of curing. In all samples,

ordinary cement hydrates, ettringite ($Ca_6(Al(OH)_6)_2(SO_4)_3 \cdot 26H_2O$) (PDF 41-1451) and portlandite ($Ca(OH)_2$) (PDF 84-1271) were identified. Additionally, unhydrated calcium silicates (C_3S) (PDF 00-055-0739), brownmillerite C_4AF (PDF 00-030-0226) and calcite ($CaCO_3$) (PDF 5-586) were found in the samples. The observed differences are limited to variations in the relative intensities of the diffraction peaks corresponding to unhydrated phases and hydration products. At both hydration ages, the samples with the additive exhibited less pronounced portlandite and unhydrated calcium silicate peaks compared to those in the reference OPC sample.

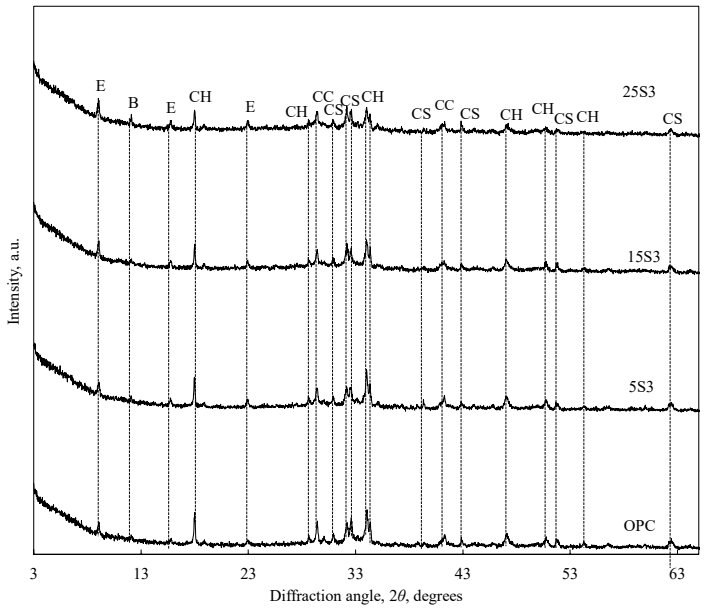

(**a**)

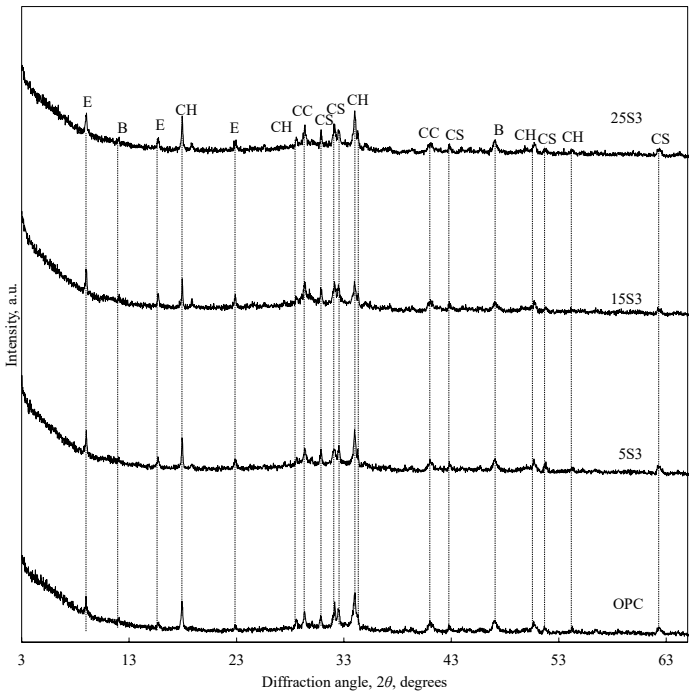

(**b**)

Figure 9. The XRD analysis curves of samples after (**a**) 7 days and (**b**) 28 days of hydration. Indexes: E—ettringite; CH—portlandite; B—brownmillerite; CS—calcium silicates, CC—calcite.

The DSC curves obtained for the samples after 7 and 28 days of aging are presented in Figure 10, and the corresponding thermogravimetric (TG) analyses are shown in Figure 11. All DSC thermograms display three well-defined endothermic peaks located within the temperature intervals of 90–270 °C, approximately 450 °C, and 570–750 °C. The initial endothermic effect is associated with the dehydration of calcium silicate hydrates (C–S–H), calcium aluminate hydrates, and ettringite. The peak near 450 °C corresponds to portlandite dehydroxylation, while the high-temperature peak observed between 570 °C and 750 °C is attributed to the decomposition of carbonates generated by the carbonation of the samples [34]. Alongside these endothermic peaks in the DSC curves of samples with additives, an exothermic peak at ~830 °C is observed. This peak is attributed to the formation of wollastonite ($CaSiO_3$) through the crystallization of semicrystalline or amorphous calcium silicate hydrates at this temperature [35].

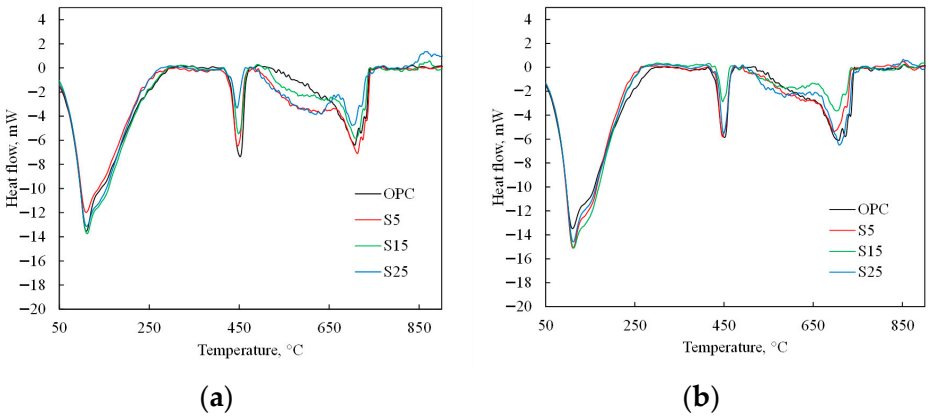

Figure 10. DSC analysis curves: (**a**) 7 and (**b**) 28 days of curing.

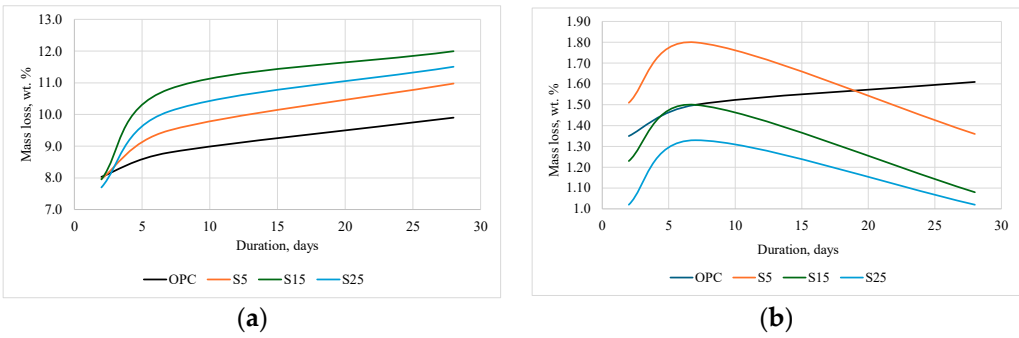

Figure 11. TG analysis curves for (**a**) a temperature range of 90–270 °C; (**b**) at ~450 °C.

All curves exhibit a generally similar shape; however, noticeable differences in their peak intensities are observed. For both curing durations, the intensity of the first endothermic peak, corresponding to the decomposition of the main cement hydration products, increases with the addition of NESW, indicating a direct relationship between additive content and peak magnitude. On the contrary, the endothermic peak associated with portlandite dehydroxylation is more pronounced in the OPC sample and in the S5 sample, and progressively decreases as the proportion of the additive increases.

Meanwhile, the intensity of the calcite decomposition peaks does not show a clear trend, except that after 28 days of hydration, the DSC peaks of the samples with additives are of lower intensity than the OPC sample. The lower degree of carbonation of the samples with additives may be related to the lower amount of portlandite (Figure 11b), which can react with atmospheric CO_2.

The results of the thermogravimetric analysis (TG) are presented in Figure 11. After 2 days of hydration, the mass loss recorded within the 90–270 °C range was quite similar

for all samples. Meanwhile, in the portlandite decomposition region (~450 °C), the greatest mass loss occurred in the S5 and OPC samples. Extending the hydration period to 7 days led to a consistent increase in mass loss within the 90–270 °C range for all samples, but the slowest growth observed in the OPC sample. A similar trend was observed near 450 °C. The increase in mass loss was more pronounced in mixtures containing the NESW additive than in the OPC reference. After 28 days of hydration, mass loss within the 90–270 °C range (Figure 11a) increased further in all samples. It should be noted that the samples incorporating the additive exhibited significantly higher values (10.98–12.00%) than the pure Portland cement sample (9.9%). A distinct difference was observed near 450 °C (Figure 11b), where portlandite decomposition occurred. At this stage, the mass loss associated with portlandite decomposition increased in OPC but decreased markedly in additive-containing samples, indicating the onset of pozzolanic reactions consuming portlandite.

The results of this section explain the results of the compressive strength of the tested samples. After two days of hardening, the amount of conventional cement hydrates (C–S–H, calcium aluminate hydrates, and ettringite) in all samples is similar. However, in OPC and S5, which had the highest compressive strength after two days of curing, a higher amount of portlandite formed was found. Meanwhile, after 28 days of curing, a higher amount of cement hydrates (mainly calcium silicate hydrates), was found in all samples with the NESW additive. The fact that, due to the pozzolanic reaction, C–S–H is formed is confirmed not only by TG analysis data, but also by the exothermic peak visible in the DSC curves. A higher content of calcium silicate hydrates in hardened cement stone leads to the improved strength and durability of cementitious materials [36,37].

In summary, the results of the research indicate that NESW is a very effective supplementary cementitious material. Only a few known SCMs can replace as much as 25% by weight of Portland cement. The effect of NESW on cement properties is comparable to that of widely used SCMs such as silica fume or metakaolin [22,34]. The use of Epsom salt production waste would not only reduce environmental pollution, but also expand the nomenclature of waste suitable for use in the cement industry.

4. Conclusions

- Epsom salt production waste consists of irregularly shaped sharp-edged amorphous materials with crystalline antigorite and magnetite impurities. It is an acidic material with a pH of 3.47.
- ESW can be neutralized with lime milk, and the water/solid material (W/S) ratio does not have a decisive influence on the neutralization process. After neutralization, the ESW becomes a non-acidic material with a pH value of 7.5, because during neutralization, the acidic components are bound to neutral compounds that do not settle on the surface of the ESW material, but pass into the liquid medium.
- Neutralized Epsom salt production waste (NESW) is characterized by very high pozzolanic activity (1085 mg CaO/g). NESW results in a slight increase in water consumption to achieve a normal consistency in cement pastes and a modest extension of the setting time of Portland cement paste.
- The addition of NESW accelerates the initial hydration of Portland cement and induces a strong pozzolanic reaction, clearly observable after 28 days of hydration.
- NESW is a very effective supplementary cementitious material, and can replace as much as 25 wt.% of Portland cement without reducing the strength class of Portland cement.

Author Contributions: Conceptualization, R.K., A.Z. and I.B.; methodology, R.K., A.Z. and I.B.; software, A.Z. and I.B.; validation, R.K., A.Z. and I.B., formal analysis, R.K. and A.Z.; investigation, R.K., A.Z. and I.B.; resources, R.K., A.Z. and I.B.; data curation, R.K., A.Z. and I.B.; writing—original

draft preparation, R.K. and A.Z.; writing—review and editing, R.K.; visualization R.K., A.Z. and I.B.; supervision, R.K. All authors have read and agreed to the published version of the manuscript.

Funding: This research received no external funding.

Data Availability Statement: The data presented in this study are available on request from the corresponding author.

Conflicts of Interest: The authors declare no conflicts of interest.

Abbreviations

The following abbreviations are used in this manuscript:

OPC	Ordinary Portland cement
SCM	Supplementary cementitious materials
C–S–H	Calcium silicate hydrates
ESW	Epsom salt production waste
DSC	Differential scanning calorimetry
TG	Thermogravimetric analysis
STA	Simultaneous thermal analysis
XRD	X-ray diffraction analysis
XRF	X-ray fluorescence analysis
SEM	Scanning electron microscope
IC	Isothermal calorimetry analysis
NESW	Neutralized Epsom salt production waste
W/S	water/solid material ratio
C3S	Calcium silicates
C4AF	Brownmillerite

References

1. Ige, O.E.; Kabeya, M. Decarbonizing the Cement Industry: Technological, Economic, and Policy Barriers to CO_2 Mitigation Adoption. *Clean Technol.* **2025**, *7*, 85. [CrossRef]
2. Li, G.; Zhou, C.; Ahmad, W.; Usanova, K.I.; Karelina, M.; Mohamed, A.M.; Khallaf, R. Fly Ash Application as Supplementary Cementitious Material: A Review. *Materials* **2022**, *15*, 2664. [CrossRef]
3. Chen, B.; Perumal, P.; Illikainen, M.; Ye, G. A Review on the Utilization of Municipal Solid Waste Incineration (MSWI) Bottom Ash as a Mineral Resource for Construction Materials. *J. Build. Eng.* **2023**, *71*, 106386. [CrossRef]
4. Hansted, F.A.S.; Mantegazini, D.Z.; Ribeiro, T.M.; Gonçalves, C.E.C.; Balestieri, J.A.P. A mini-review on the use of waste in the production of sustainable Portland cement composites. *Waste Manag. Res.* **2022**, *41*, 828–838. [CrossRef] [PubMed]
5. Ndahirwa, D.; Zmamou, H.; Lenormand, H.; Leblanc, N. The role of supplementary cementitious materials in hydration, durability and shrinkage of cement-based materials, their environmental and economic benefits: A review. *Clean. Mater.* **2022**, *5*, 100123. [CrossRef]
6. Ma, M.; Tam, V.W.Y.; Le, K.N.; Osei-Kyei, R. Factors affecting the price of recycled concrete: A critical review. *J. Build. Eng.* **2022**, *46*, 103743. [CrossRef]
7. Al-Hellali, N.; Bengtsson, M.; Nagy, A.; Sadagopan, M. Glass waste as a supplementary cementitious material in climate reduced concrete—A review. *Nord. Concr. Res.* **2025**, *72*, 167–181. [CrossRef]
8. Xiong, Y.; Zhang, A.; Zhao, Y.; Xu, Q.; Ding, Y. A mini review on sewage sludge and red mud recycling for thermal energy storage. *Energies* **2024**, *17*, 2079. [CrossRef]
9. Fode, T.A.; Jande, Y.A.C.; Kivevele, T. Effects of different supplementary cementitious materials on durability and mechanical properties of cement composite–comprehensive review. *Heliyon* **2023**, *9*, e17924. [CrossRef]
10. Ahmed, A. Assessing the effects of supplementary cementitious materials on concrete properties: A review. *Discov. Civ. Eng.* **2024**, *1*, 145. [CrossRef]
11. Gao, S.; Chu, H.; Shi, W.; Wang, F.; Jiang, J. Utilization of municipal solid waste incineration fly ash in ecological concrete and pavement bricks: Mechanical properties and environmental impact. *Case Stud. Constr. Mater.* **2024**, *21*, e03999. [CrossRef]

12. Kaminskas, R.; Barauskas, I. Influence of pozzolana on sulfate attack of cement stone affected by chloride ions. *Mater. Struct.* **2014**, *47*, 1901–1910. [CrossRef]
13. Hu, L.; He, Z.; Zhang, S. Sustainable use of rice husk ash in cement-based materials: Environmental evaluation and performance improvement. *J. Clean. Prod.* **2020**, *264*, 121744. [CrossRef]
14. Castellanos, N.T.; Agredo, J.T. Using spent fluid catalytic cracking (FCC) catalyst as pozzolanic addition—A review. *Ing. Investig.* **2010**, *30*, 35–42. [CrossRef]
15. Zito, S.V.; Irassar, E.F.; Rahhal, V.F. Recycled construction and demolition waste as supplementary cementing materials in eco-friendly concrete. *Recycling* **2023**, *8*, 54. [CrossRef]
16. Doneliene, J.; Eisinas, A.; Baltakys, K.; Bankauskaite, A. The effect of synthetic hydrated calcium aluminate additive on the hydration properties of OPC. *Adv. Mater. Sci. Eng.* **2016**, *2016*, 3605845. [CrossRef]
17. Kaminskas, R.; Savickaite, B.; Eisinas, A. Hydrothermally treated cement bypass dust as a supplementary cementitious material. *Sustainability* **2025**, *17*, 6757. [CrossRef]
18. Auyeshov, A.; Arynov, K.; Yeskibayeva, C.; Ibrayeva, A.; Zhumadildayeva, A. Efficient production of high-purity magnesium hydroxide from serpentinite. *Molecules* **2025**, *30*, 3484. [CrossRef]
19. Zhao, Q.; Liu, C.-J.; Jiang, M.-F.; Saxén, H.; Zevenhoven, R. Preparation of magnesium hydroxide from serpentinite by sulfuric acid leaching for CO_2 mineral carbonation. *Miner. Eng.* **2015**, *79*, 116–124. [CrossRef]
20. Romão, I.; Gando-Ferreira, L.M.; Zevenhoven, R. Separation and recovery of valuable metals extracted from serpentinite during the production of $Mg(OH)_2$ for CO_2 Sequestration. *Miner. Eng.* **2015**, *77*, 25–33. [CrossRef]
21. Hamada, H.M.; Abed, F.; Beddu, S.; Humada, A.M.; Majdi, A. Effect of volcanic ash and natural pozzolana on mechanical properties of sustainable cement concrete: A comprehensive review. *Case Stud. Constr. Mater.* **2023**, *19*, e02425. [CrossRef]
22. Jeong, Y.; Kang, S.-H.; Kim, M.O.; Moon, J. Acceleration of cement hydration from supplementary cementitious materials: Performance comparison between silica fume and hydrophobic silica. *Cem. Concr. Compos.* **2020**, *112*, 103688. [CrossRef]
23. Shanks, B.; Howe, C.; Draper, S.; Wong, H.; Cheeseman, C. Production of low-carbon amorphous SiO_2 for use as a supplementary cementitious material and nesquehonite from olivine. *Mater. Lett.* **2024**, *361*, 136133. [CrossRef]
24. Lin, Y.; Alengaram, U.J.; Ibrahim, Z. Effect of treated and untreated rice husk ash, palm oil fuel ash, and sugarcane bagasse ash on the mechanical, durability, and microstructure characteristics of blended concrete–a comprehensive review. *J. Build. Eng.* **2023**, *78*, 107500. [CrossRef]
25. Zulumyan, N.; Isahakyan, A.; Beglaryan, H.; Melikyan, S. A study of thermal decomposition of antigorite from dunite and lizardite from peridotite. *J. Therm. Anal. Calorim.* **2018**, *131*, 1201–1211. [CrossRef]
26. *EN 196-3:2016*; Methods of Testing Cement. Determination of Setting Times and Soundness. European Committee for Standardization (CEN): Brussels, Belgium, 2016.
27. *EN 196-1:2016*; Methods of Testing Cement. Determination of Strength. European Committee for Standardization (CEN): Brussels, Belgium, 2016.
28. *NF P18-513:2012*; Metakaolin. Pozzolanic Addition for Concrete. Association Française de Normalisation: La Plaine Saint-Denis, France, 2012.
29. Quarcioni, Y.; Chotoli, V.A.F.F.; Coelho, A.C.V.; Cincotto, M.A. Indirect and direct chapelle's methods for the determination of lime consumption in pozzolanic materials. *Rev. IBR. Estrut. Mat.* **2015**, *8*, 1–7. [CrossRef]
30. Hesse, C.; Goetz-Neunhoeffer, F.; Neubauer, J.A. New Approach in Quantitative In-Situ XRD of Cement Pastes: Correlation of Heat Flow Curves with Early Hydration Reactions. *Cem. Concr. Res.* **2011**, *41*, 123–128. [CrossRef]
31. Pichler, C.; Perfler, L.; Lackner, R. Deconvolution of main hydration kinetic peaks in properly sulfated Portland cements with boundary nucleation and growth models and relation to early-age concrete strength development. *Constr. Build. Mater.* **2022**, *348*, 128602. [CrossRef]
32. Scrivener, K.L.; Juilland, P.; Monteiro, P.J.M. Advances in understanding hydration of Portland cement. *Cem. Concr. Res.* **2015**, *78*, 38–56. [CrossRef]
33. *EN 197-1:2011*; Cement–Part 1: Composition, Specifications and Conformity Criteria for Common Cements. European Committee for Standardization (CEN): Brussels, Belgium, 2011.
34. El-Diadamony, H.; Amer, A.A.; Sokkary, T.M.; El-Hoseny, S. Hydration and Characteristics of Metakaolin Pozzolanic Cement Pastes. *HBRC J.* **2018**, *14*, 150–158. [CrossRef]
35. Gineika, A.; Siauciunas, R.; Baltakys, K. Synthesis of wollastonite from AlF3-rich silica gel and its hardening in the CO_2 atmosphere. *Sci. Rep.* **2019**, *9*, 18063. [CrossRef] [PubMed]

36. Kumar, A.; Walder, B.J.; Kunhi Mohamed, A.; Hofstetter, A.; Srinivasan, B.; Rossini, A.J.; Scrivener, K.; Emsley, L.; Bowen, P. The atomic-level structure of cementitious calcium silicate hydrate. *J. Phys. Chem. C* **2017**, *121*, 17188–17196. [CrossRef]
37. Miah, M.J.; Huaping, R.; Paul, S.C.; Babafemi, A.J.; Li, Y. Long-term strength and durability performance of eco-friendly concrete with supplementary cementitious materials. *Innov. Infrastruct. Solut.* **2023**, *8*, 255. [CrossRef]

Disclaimer/Publisher's Note: The statements, opinions and data contained in all publications are solely those of the individual author(s) and contributor(s) and not of MDPI and/or the editor(s). MDPI and/or the editor(s) disclaim responsibility for any injury to people or property resulting from any ideas, methods, instructions or products referred to in the content.